Sequential Self-Folding of Shape Memory Polymer Sheets by Laser Rastering Toward Origami-Based Manufacturing

Moataz Abdulhafez
Department of Industrial Engineering,
University of Pittsburgh,
Pittsburgh, PA 15261
e-mail: MMA89@pitt.edu

Joshua Line
Department of Industrial Engineering,
University of Pittsburgh,
Pittsburgh, PA 15260
e-mail: jal257@pitt.edu

Mostafa Bedewy[1]
Department of Industrial Engineering,
Department of Chemical and
Petroleum Engineering,
Department of Mechanical Engineering and
Materials Science,
University of Pittsburgh,
Pittsburgh, PA 15261
e-mail: mbedewy@pitt.edu

Origami-based fabrication strategies open the door for developing new manufacturing processes capable of producing complex three-dimensional (3D) geometries from two-dimensional (2D) sheets. Nevertheless, for these methods to translate into scalable manufacturing processes, rapid techniques for creating controlled folds are needed. In this work, we propose a new approach for controlled self-folding of shape memory polymer sheets based on direct laser rastering. We demonstrate that rapidly moving a CO_2 laser over pre-strained polystyrene sheets results in creating controlled folds along the laser path. Laser interaction with the polymer induces localized heating above the glass transition temperature with a temperature gradient across the thickness of the thin sheets. This gradient of temperature results in a gradient of shrinkage owing to the viscoelastic relaxation of the polymer, favoring folding toward the hotter side (toward the laser source). We study the influence of laser power, rastering speed, fluence, and the number of passes on the fold angle. Moreover, we investigate process parameters that produce the highest quality folds with minimal undesired deformations. Our results show that we can create clean folds up to and exceeding 90 deg, which highlights the potential of our approach for creating lightweight 3D geometries with smooth surface finishes that are challenging to create using 3D printing methods. Hence, laser-induced self-folding of polymers is an inherently mass-customizable approach to manufacturing, especially when combined with cutting for integration of origami and kirigami. [DOI: 10.1115/1.4050463]

Keywords: advanced materials and processing, laser processes, micro- and nano-machining and processing, sheet and tube metal forming

1 Introduction

Directed self-folding of 2D stock materials to create complex 3D geometries is an attractive pathway toward manufacturing functional structures at different length scales. This origami-based approach of self-folding is observed in nature at different length scales ranging from nanometers to meters. Organic molecules [1], insects [2], brain tissue [3], and tree leaves [4] are all observed to use folding techniques for producing 3D structures that underlie their function. Similarly, engineered origami and nature inspired foldable structures have found applications in areas like robotics [5], implantable devices [6], sensors, actuator [6], aerospace [7], and battery development [8].

The main element of a self-folding technique is the used material which has to exhibit a change in geometry as a response to a stimulus like light [9–11], heat [5,9,10], and surface tension [11]. The accumulation of such spatially varying responses to stimuli results in controlled folding at desired locations. Polymers are ideal as a self-folding material since they can be durable, low-cost, lightweight, bio-compatible and can be designed to be stimulus responsive, such as in the case of shape memory polymers (SMP). A polymer can be programed by prestraining at high temperature, followed by cooling below the glass transition temperature. Hence, pre-strained polymer sheets are a widely used material in self-folding research since they are a low-cost and versatile material to induce self-folding from the macroscale to the microscale. When heated, localized thermal gradients in the material lead to a shrinkage across the thickness of the sheet which induces instant folding in the sheet [9,12,13].

Different methods have been proposed in literature to induce folding stimuli of both non-SMP sheets and SMP sheets, including focused or unfocused light radiation [12,14,15], heat conduction through resistive wires [5,9,10], microwave irradiation [16], uniform by ovens or air guns [13,17], and surface tension [11] as illustrated in Fig. 1. In addition to differences in stimuli and heating method, techniques can also differ based on whether the folds are made in a sequential or a simultaneous manner. Liu et al. [12] initially demonstrated the self-folding of pre-strained films by using local light absorption generated from an unfocused IR light bulb that heats pre-defined hinges patterned by desktop printing. Recently, Lee [20,21] has developed a technique using curvilinear strain engineering to create complex 3D geometries and curvatures from 2D inked polymer sheets, subject to unfocused light. Felton et al. [13] developed a method where composites of pre-strained polymer hinges bonded to paper are activated to fold by joule heating via resistive circuits at the hinges. Elsisy et al. [9,10] developed a technique using resistive heating ribbons to locally heat the pre-strained polymer sheets and demonstrated that changing the composite layer combination can be utilized to control the direction of hinge fold in the structure. Another noncontact technique developed utilizes microwave absorbing ink [16] to define the hinges on microwave transparent pre-strained polymer. When the sheet is subject to microwaves, the ink patterns heat up remotely, leading to hinge folding. To demonstrate selective sequential folding using unfocused light, Liu et al. [15] used printed ink of different colors to define the hinges on the surface of the polymer sheets. This enabled controlling the amount of absorbed light based on the wavelength of the used light and the color of the ink, hence achieving selective folding. In addition to

[1]Corresponding author.

Manuscript received November 27, 2020; final manuscript received February 19, 2021; published online April 1, 2021. Assoc. Editor: Y. Lawrence Yao.

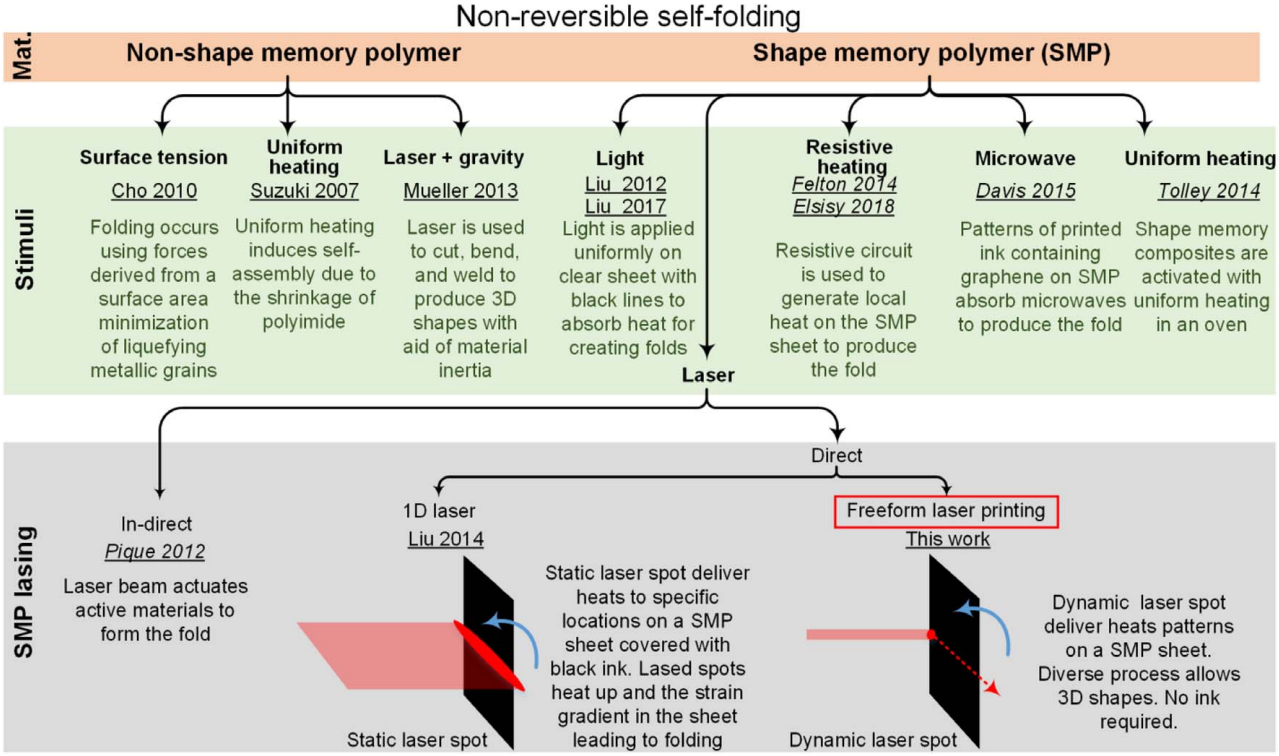

Fig. 1 Illustration of different methods of inducing self-folding of polymers based on external stimuli [5,9,11–19], highlighting the unique freeform direct-write capability of our new approach

self-folding using unfocused light, direct local heating of the pre-strained films has also been demonstrated using laser to induce folding [22] by focusing a continuous-wave (CW) laser with an elongated beam shape using a cylindrical lens. In that method however, the shaped laser spot is fixed and is wider than the used polymer strip as illustrated in Fig. 1. Indirect laser heating was also demonstrated in which the laser was used to heat the sample substrate instead of the sample itself [18]. Here, we propose a scalable approach for controlled self-folding of shape memory polymers based on laser rastering. Localized heating is achieved by moving laser to deliver controlled energy across the rastering path. This is in contrast to prior work on using a stationary laser spot with a rectangular shape described earlier as illustrated in Fig. 1. Our approach allows the accurate control of the spatiotemporal delivery of heat as a function of laser power, speed and number of passes along designed paths on the polymer, which enables control of fold angle and quality. Our results demonstrate that this approach can used to create complex three-dimensional shapes. Hence, it paves the way for developing unique manufacturing capabilities in creating functional parts that require complex 3D geometries and high surface quality.

2 Materials and Methods

2.1 Sample Preparation. Commercially available sheets of pre-strained polystyrene sheets are used in this study (Grafix® Black Shrink Film, thickness 0.3 mm, bi-axially contract 55% approximately when heated above the glass transition temperature ($T_g = 103$ °C) were used in this study. These sheets are known to have shape memory properties. This is achieved by heating the polymer above its glass transition temperature (T_g), stretching, and then cooling below T_g to preserve its shape. When the material is heated above the T_g, the preserved stresses are released. These sheets were used in previous work for studying self-folding using different stimuli, and their properties are described in detail in other work [12,13,16,19,22].

The sheets were cut down to sample sizes of 10 × 20 mm using a ruler and scissors. A protractor and ruler were used to measure the bending angle of the sheets after subjecting them to laser heating. Masking tape and Kapton tape were used to secure the samples to the laser platform, as shown in Figs. 2(*a*) and 2(*b*).

2.2 Laser System. The laser used is a CW CO_2 laser system (Full Spectrum Laser Pro-Series 20 × 12, 1.5 in. focus lens) with 10.6 μm wavelength and 35 W power from the laser. The black polystyrene used in this study is highly absorbing to 10.6 μm laser light. The laser power can be adjusted by changing the laser current through pulse width modulation. We measure the laser power at different currents using a CO_2 laser power meter (HLP-200, Changchun Laser Optoelectronics Technology Co., Ltd.). The beam radius was measured based on ($1/e^2$) of the maximum intensity (w_y, w_x) at different distances (z) from the beam waist using the knife-edge method [23], where we assume single mode operation (TEM00) with a Gaussian beam profile. Using this technique, the beam radius at the beam waist (w_{ox}, w_{oy}), based on a Gaussian beam assumption, was determined to be 125.8 μm in the x direction and 84 μm in the y direction. The experimental beam radius in the x direction and the estimated beam shape is shown in Fig. 2(*c*). Using the beam size and measured laser power, the flux at different defocus values is shown in Fig. 2(*d*).

Additionally, the laser is equipped with an air assist system, which is an air nozzle that is aligned with the laser beam that blows air onto the sample. The function of the air assist is to prevent overheating of the sample and to clear the lasing path from any debris or smoke.

A power (P) ranges of 0.14–28 W was used in our experiments in order to control the folding process. A speed (v) range of 108–508 mm/s and a fixed spot size (w) of 1 mm were used as well. Within this range of parameters, we were able to control how much energy and fluence were applied to the sample during folding.

2.3 Experimental Setup. The prepared samples were placed on an aluminum grating within the laser system as illustrated in

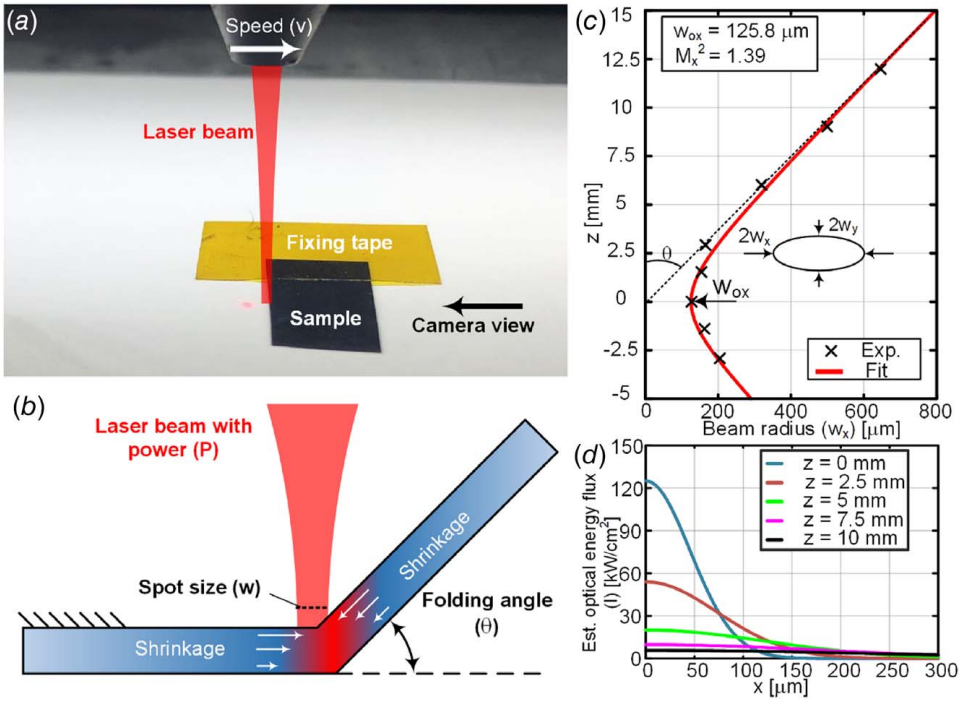

Fig. 2 (*a*) Photograph of the laser processing setup, showing the laser objective lens and the sample with annotation for lasing direction, laser beam, and camera view for videography results shown in this paper. (*b*) Schematic of the folding process showing the gradient of shrinkages, which results from the viscoelastic relaxation across the thickness of the pre-strained sheet having a gradient of temperature. (*c*) Experimental points representing the estimated laser beam profile along the lasing direction *x* using the knife-edge technique, along with the profile of the fitted Gaussian beam illustrating the divergence of the beam away from the beam waist. The resulting beam spot in the *x* direction is estimated to be $2w_{ox} = 251.6\ \mu m$. (*d*) Estimated optical flux along the x direction at constant power ($P = 22.5$ W), showing the change of beam intensity with *z* (i.e., with changing spot size by defocusing the beam).

Figs. 2(*a*) and 2(*b*). The samples were secured by using a piece of masking tape or Kapton tape to hold the sample in place during the experiment. When the laser is subject to laser heating, the polymer strips would bend with an angle (θ), as illustrated in Fig. 2(*b*), that is measured with a protractor with respect to the sheets original position. To control the energy delivered for folding, we can control laser power (P), speed (v), and number of lasing passes. Upon completing a forward path, the lasing head would decelerate, switch direction, and conduct a return path till the number of passes is completed. Additionally, we test the influence of turning the air assist on or off since the blown air would create some forces on the bending strips while lasing and also cool off the lased lines.

2.4 In Situ Videography and Ex Situ Imaging. Microscope cameras (Celestron Handheld Digital Microscope Pro) were used for imaging of the samples and videography during the lasing process. Scanning electron microscopy (SEM) images of the folds were completed on a Zeiss SIGMA VP Field emission scanning electron microscope. The samples were sputter coated with platinum and then imaged with a beam with an accelerating voltage of 2 kV.

3 Results and Discussion

3.1 Influence of Power and Speed With Air Assist On. In this experimental study, the influence of power and speed with the air assist on is tested. In the experiment, a power range ($P = 0.1$–9 W) with a speed range ($v = 107$–500 mm/s) were investigated at a fixed spot size ($2w_x = 1$ mm) for nine passes. Multiple passes are conducted in rapid succession, wherein the lasing head abruptly decelerates upon completing a forward path and switch direction to conduct a return path at the same speed (v). The stopping time is estimated to be small compared with the lasing time. The resulting folding angles are shown in Fig. 3. Folding started at powers ranging from 1.4 W to 2 W, depending on the lasing speed. The results generally show a quick increase in folding angle between powers 1–2 W. With higher speed, it is noted that

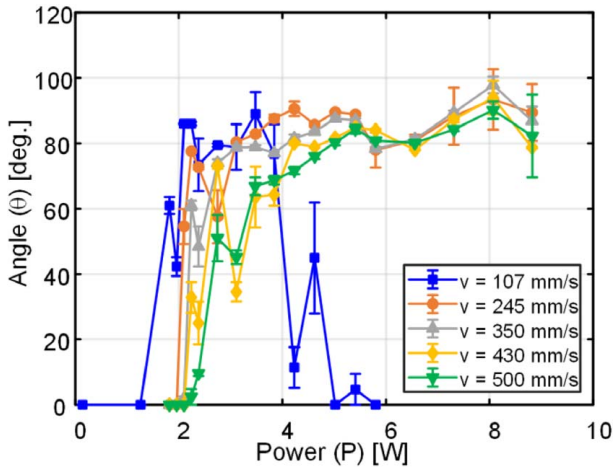

Fig. 3 The resulting folding angles generated from different power and speed combinations for the laser with the air assist on. All samples were subject to nine lasing passes. Error bars indicate standard error based on seven replications.

Fig. 4 Side view and top view images indicating the influence of laser conditions on fold distortion and quality, where too much heating leads to excessive deformation manifested as highly distorted hinges ($P = 3.5$ W, $v = 500$ mm/s, $2w_x = 1$ mm, $n = 9$) and ($P = 3.5$ W, $v = 107$ mm/s, $2w_x = 1$ mm, $n = 9$) were imaged using SEM as well

the transition occurs more slowly. In addition, in the lowest speed case ($v = 107.5$ mm/s), the folding increases and then drop at powers beyond 3 W, indicating that excessive deformation or cutting damage has occurred.

One advantage of using the air assist is that since the airflow has a cooling effect on the polymer samples, a larger power range can be explored and a higher range of high-quality folds can be achieved. For example, when the samples are subject to excessive laser fluence, folding can occur but it is accompanied by excessive deformation and distortion to the fold geometry locally at the hinge. Thes undesired effects might lead to issues of reduced repeatability and compromised structural integrity of the resulting 3D structures. A juxtaposition of different fold geometries is shown in Fig. 4, illustrating that there is a wide range of shapes of folds that occur at the different combinations of power and speed. While some lasing conditions lead to large angle folding, some of the folds are too distorted. This is why characterizing the quality of the fold by optical imaging is an important complement to the measurement of fold angle. Importantly, it is noted that from our observation, we find that some conditions can achieve both large folding angles and minimal distortion to fold geometry, as shown in Fig. 4.

In addition to optical imaging, we use SEM to further investigate fold surface quality and local distortion. Our SEM images show the effect of overheating (at conditions of lower laser speed) on compromising fold quality as shown in Figs. 5(*a*) and 5(*b*). The local shrinkage and excessive material flow are visible.

3.2 Influence of Power and Speed With Air Assist Off. We also investigate the influence of power and speed in the absence of air assist, by varying laser power and speed while maintaining a constant spot size, with the air assist off. In this study, a power range ($P = 0.1$–5 W) is tested with a speeds ranging from 107.5 to 500 mm/s and a fixed spot size ($2w_x = 1$ mm) for nine passes. With the air assist off, the polymer samples were subject to higher fluence for a small power range, as compared with the air assist mode. Moreover, turning of the air flow also eliminated the resistance force pushing down on the sample.

Results shown in Fig. 6 indicate that folding started at $P = 0.1$ W at the lowest speed ($v = 107.5$ mm/s), much lower than with the similar conditions with air assist on, demonstrating the effect of the lower air pressure and no air cooling on the folding.

In the cases with lasing speeds $v = 107.5$ mm/s and 245.5 mm/s, folding angles are noted to drop beyond $P = 1.5$ W and 3.5 W, respectively, indicating excessive heating that cause too much flow of material or melting of the polymer in some cases. At higher speeds, little change is noted between the folding angle at different speeds. In these cases, folding starts at 1.5 W lasing

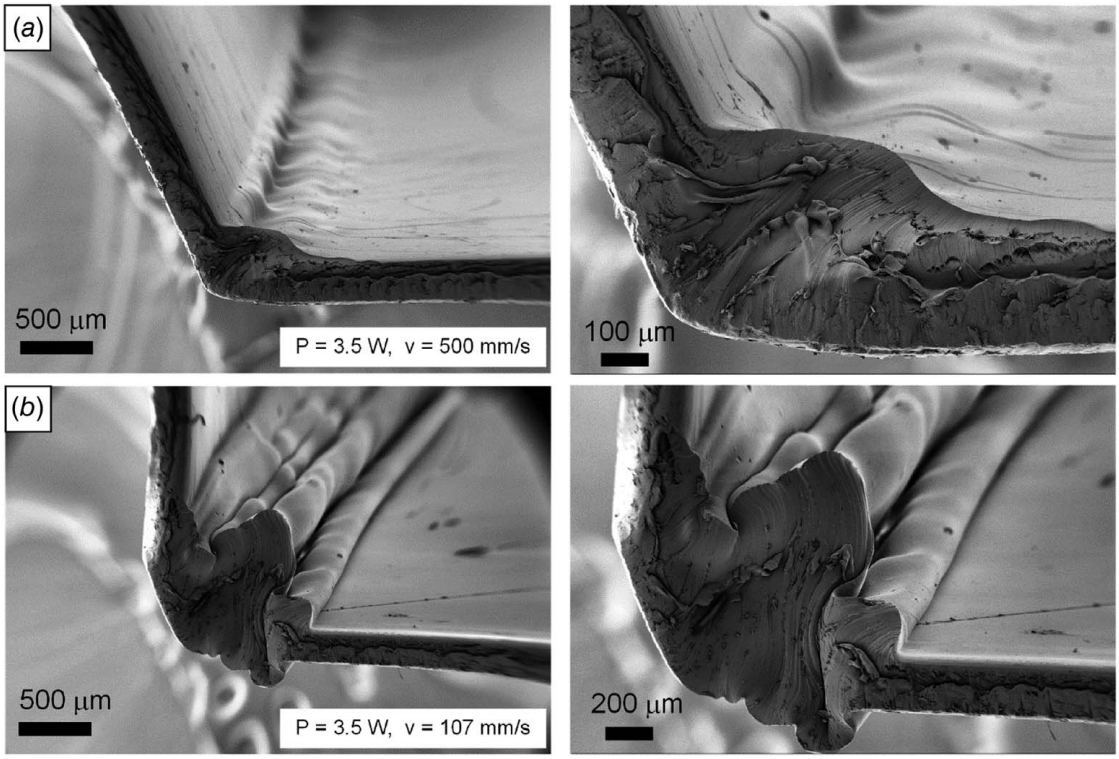

Fig. 5 (*a*) SEM image of fold with minimal hinge distortion illustrating the folding and shrinkage pattern at the edge and at the fold ($P = 3.5$ W, $v = 500$ mm/s, $2w_x = 1$ mm, $n = 9$) and (*b*) SEM image of fold with excessive fold distortion ($P = 3.5$ W, $v = 107$ mm/s, $2w_x = 1$ mm, $n = 9$)

power, which transitions with increasing power till an average folding angle of 90 deg is reached at a power of 5 W.

3.3 Influence of Number of Lasing Passes. To explore the effect of the number of passes on the folding angle, the number of passes was varied between 1 and 10 passes at two levels of power ($P = 2.4$ W and $P = 5.8$ W) and a fixed speed ($v = 350$ mm/s), fixed spot size and air assist on.

Real-time monitoring of folding angle after each pass is achieved by employing in situ videography. Results where images of the folding are recorded with number of passes are shown in Fig. 7. It is noteworthy that after one lasing pass there is little folding,

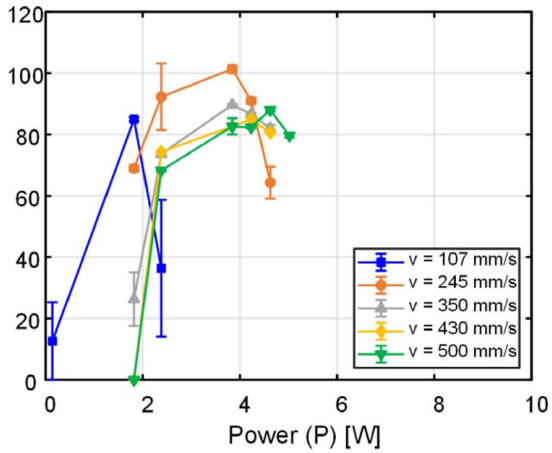

Fig. 6 The resulting folding angles generated from different power and speed combinations for the laser with the air assist off. All samples were subject to nine lasing passes. Error bars indicate standard error based on seven replications.

but with subsequent folds, the folding angle increases incrementally until it reaches an average value of around 30 deg at these conditions ($P = 3.5$ W, $v = 430$ mm/s, $2w_x = 1$ mm). This indicates that the cumulative effect of incrementally adding small energy doses can gradually increase the temperature at the hinge to activate the folding without excessively damaging the hinge. The quantitative results for folding angle dependence on number of passes are presented in Fig. 8. For the low power case in Fig. 8(*a*), it is noted that no folding occurs for less than five lasing passes. This implies that the temperature was not high enough to trigger folding until after the fifth pass. With increasing number of passes, the folding angle reached an average value of 8 deg. Eventually, the angle starts to drop after nine passes. For the higher power, shown in Fig. 8(*b*), folding starts after two lasing passes. Also, the fold angle increases up to an average of 90 deg which drops after the eighth pass. The nature of the process prevents lasing beyond 90 deg since the beam will be blocked by the folded side of the polystyrene sheet. The drop in angle is caused by excessive heating and material flow, as will be discussed later. As noticed from the optical and SEM imaging (Figs. 4 and 5), overheating leads to melting and excessive hinge deformation, which are undesirable. In addition to excessive material flow, more passes lead to excessive relaxation across the whole sheet and hence lower strain gradients and smaller folding angles.

3.4 Influence of Laser Power and Speed on Single Pass Folding. To gain more insight into the process fundamentals, we lase the pre-strained polystyrene for only a single pass ($n = 1$) at different values of power and speed. We also estimate the corresponding fluence at the different laser conditions to see how fluence is correlated with folding angle. The relationship between power and average fluence is shown in Fig. 9(*a*) at $2w_x = 1$ mm. The average fluence is calculated based on Gaussian beam modeling by multiplying the average estimated optical energy flux (as shown in Fig. 2(*d*)) with the laser dwell time ($t_d = 2w_x/v$). The

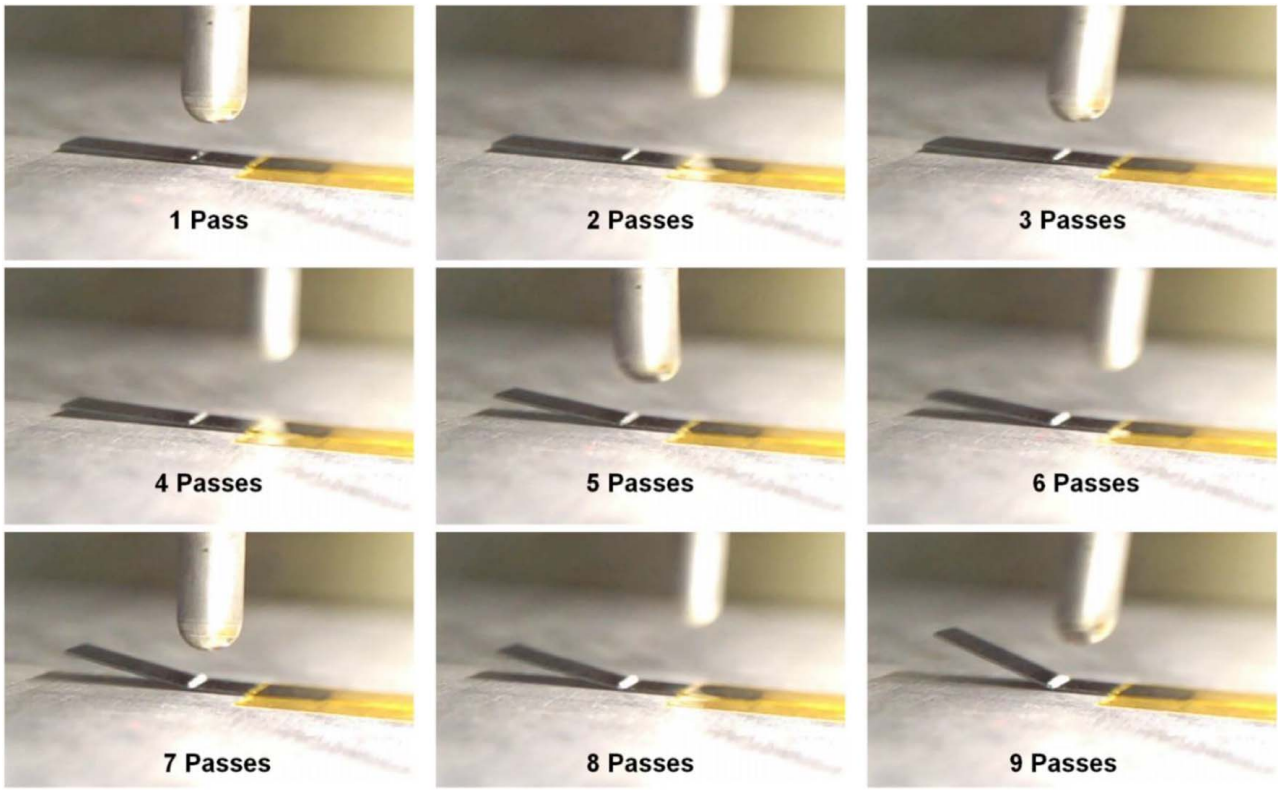

Fig. 7 Image frames from in situ videography showing the progression of folding with increasing number of lasing passes at conditions of $P = 3.5$ W, $v = 430$ mm/s, $2w_x = 1$ mm, air assist on. The sliver moving part is the laser head plunger, which is used for focusing/defocusing the laser beam on the sample before rastering.

plotted results show that the laser fluence scales linearly with power, with a higher rate of fluence increase at lower speeds. The resulting fold angles at different laser power and speed are shown in Fig. 9(*b*), with the corresponding fluence values illustrated in Fig. 9(*c*). The avg. fluence (F_{avg}) at which folding starts is plotted as a function of lasing speed in Fig. 9(*d*) as well as the dwell time for each laser conditions. For all conditions, folding does not start at $P < 8$ W and $F_{avg} < 5.2$ J/cm^2, implying that the temperature across the material resulting from these lasing conditions is not high enough to initiate folding (i.e., does not reach the glass transition temperature). It is also noted that the fluence at the initiation of folding is different for each lasing speed. At the lowest speed ($v = 250$ mm/s), the fluence at which folding starts is at $F_{avg} = 5.4$ J/cm^2, while at the highest speed ($v = 500$ mm/s), the fluence at which folding starts at $F_{avg} = 8.2$ J/cm^2. For the lowest speed (highest dwell time), an increasing trend is noticed with fluence till a maximum of 25 deg at a $F_{avg} = 13$ J/cm^2 after which the folding angle drops with increasing fluence till no folding is observed after $F_{avg} = 17$ J/cm^2. At $v = 340$ mm/s, the folding initiates at $F_{avg} = 6.8$ J/cm^2, and is followed by a monotonic increase in folding angle with average fluence with a maximum average folding angle of 37 deg at a fluence of $F_{avg} = 12$ J/cm^2. Further increase of fluence was not experimentally achievable due to laser maximum power limitations. It is expected that beyond a certain fluence values, the resulting folding angle will start to decrease, similar to the results obtained at $v = 250$ mm/s (due to overheating

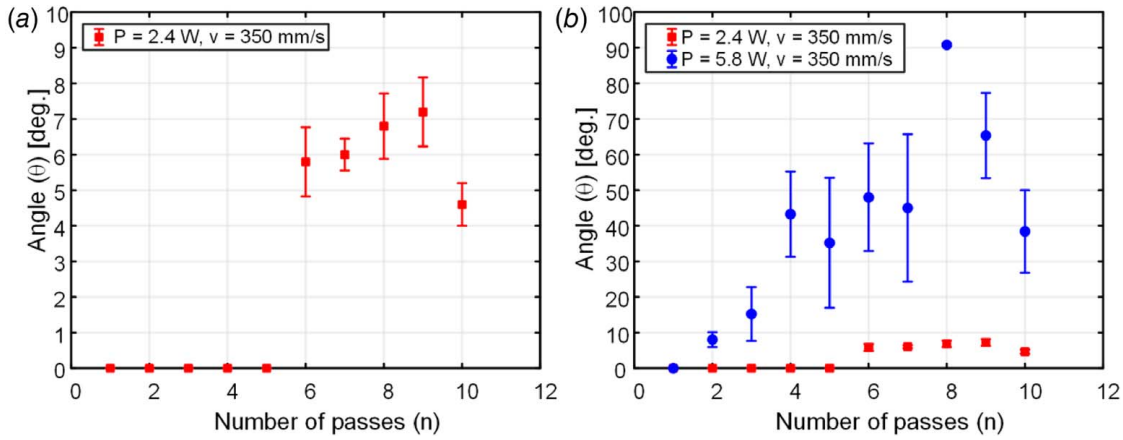

Fig. 8 (*a*) Plot showing the effect of number of passes at fixed power and speed ($P = 2.4$ W, $v = 350$ mm/s, $2w_x = 1$ mm) and (*b*) ($P = 5.8$ W, $v = 350$ mm/s, $2w_x = 1$ mm). Error bars indicate standard error based on ten replications. At eight passes for $P = 5.8$ W, $v = 350$ m/s the standard error is 0.37.

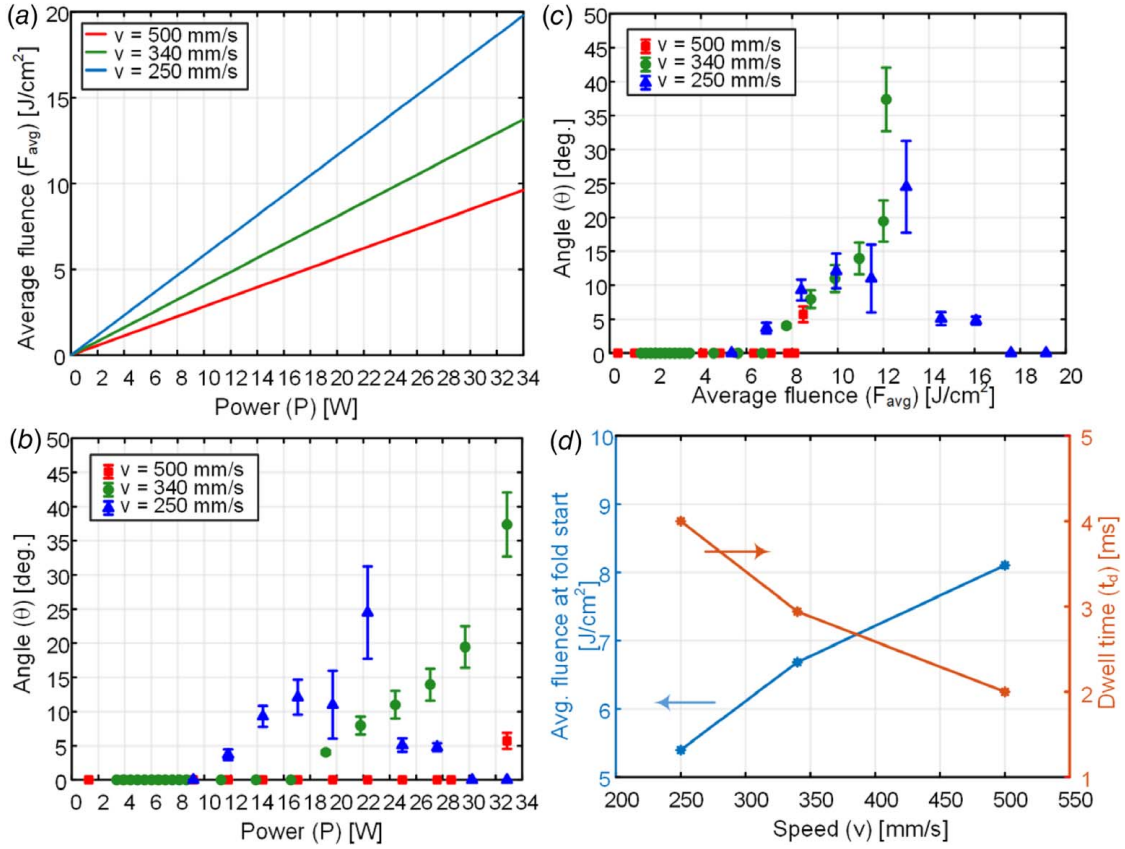

Fig. 9 ***(a)*** **Plot showing how laser power and speed affect laser fluence, (*b*) folding angle at different speeds and powers (errors bars are the standard error for sample size of 5), (c) influence of laser fluence and speed on folding angle, and (*d*) influence of speed and dwell time on the threshold fluence for folding**

as explained below). At the highest speed, the fluence needed to initiate folding is highest at $F = 8.1$ J/cm^2. Higher fluence could not be delivered due to the maximum laser power limits.

As mentioned earlier, the shrinkage of pre-strained polystyrene films is dependent on the material temperature exceeding the glass transition temperature (T_g), leading to the viscoelastic relaxation locally, which causes the folds. In this case, the resulting fold angle and speed of folding are dependent on multiple factors. The temporal and spatial temperature distributions (which depend on the laser parameters and material properties) combined with temporal viscoelastic effects (the rate of stress relaxation is also temperature dependent) dictate the observed folding. for low lasing speeds, high fluence, and long laser dwell time can lead to low or no folding, because these conditions lead to full stress relaxation of the prestrain across the polystyrene sheet without gradient of shrinkage across the thickness [hence, no folding is observed for higher power points shown in Fig. 9(*b*)]. We observe this effect experimentally at laser scanning speed at $v = 250$ mm/s, where the folding angle increased with fluence and then dropped subsequently. Excessive heating can also lead to polystyrene melting and excessive material flow, preventing high-quality folding. Future research to elucidate these interactions will focus on thermo-mechanical simulations to study how the lasing conditions interact with the viscoelastic properties of the materials and how they influence the folding dynamics.

3.5 Applications of Complex 3D Geometries. After demonstrating the ability to control both fold angle and quality of fold based on varying laser power and rastering speed, we have also shown that sequential delivery of energy through multiple lasing passes can also be used as a powerful knob to control the localized folding angle. We have combined cutting with folding to illustrate the capability of our approach to create complex 3D geometries like vertex connected triply periodic minimal surface structures which are attractive geometries for mechanical metamaterial applications [24], as shown in Fig. 10. This highlights the potential of integrating origami and kirigami [25] principles in manufacturing.

We demonstrate the robustness of the produced folds by applying a compressive load on them, as shown in Fig. 11. We show that for a load of 1 N does not damage the folds obtained at the lasing conditions of $P = 3.5$ W, $v = 500$ mm/s, $2w_x = 1$ mm, $n = 9$. In this experiment, a load is applied on top of the vertex of the fold as illustrated in Fig. 11(*a*), while the sample is mounted on a mass balance. Results show that the fold withstand the load, which the polystyrene elastically deform, and returned to its original configuration upon unloading (Fig. 11(*b*)) without any damage to the folds. Hence, the resulting geometries obtained by our laser-based folding approach are promising as a building block in a repeating architected structure for origami-based energy absorption applications [26] and origami-based cellular metamaterials [27].

Hence, our approach is promising for fabrication of lightweight polymer structures with high surface finish, which is a major advantage compared with common additive manufacturing alternatives. The reason that surface finish is much more superior in our laser-based origami approach compared with 3D printing methods is that the surface finish is dependent on the process of fabricating 2D sheets, which is a rather cost-effective and mature technology. For example, a single 8 in. × 11 in. sheet of smooth pre-strained polystyrene costs less than 0.4$. Our folding approach is also faster than typical additive manufacturing approaches such as fused deposition modeling and stereolithography, which also generating minimal waster material.

Our rastering-based approach also invites leveraging computational design tools for control of the spatiotemporal evolution of temperature for achieving desired curves and folds. Combining

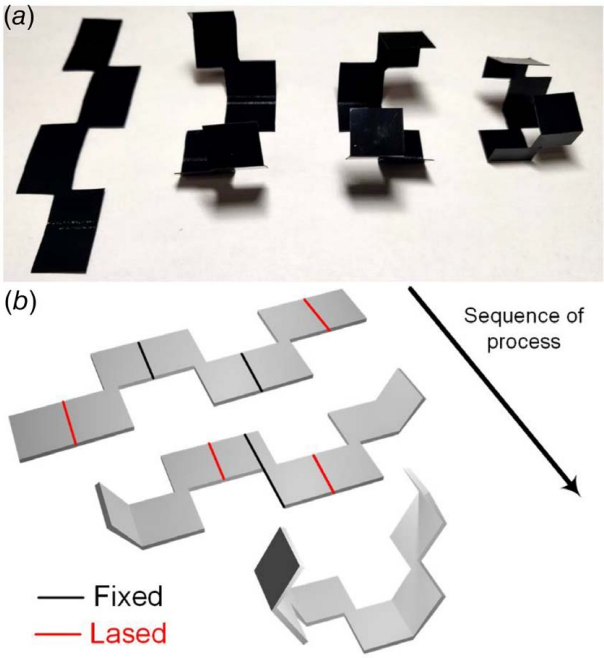

Fig. 10 (*a*) Demonstration of complex shapes such as vertex connected triply periodic minimal surface structures, created with combining cutting with the laser self-folding approach described in this work and (*b*) illustration for the sequence of lasing, with lasing paths and fixation points shown

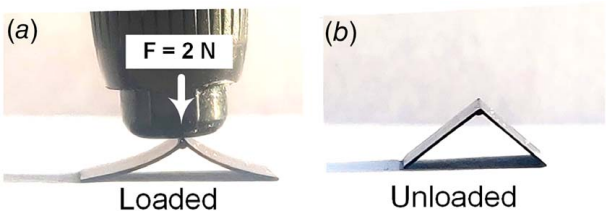

Fig. 11 Demonstration for the mechanical robustness of the folds. A compressive load of 2 N was placed on the folds (*a*). After unloading (*b*), the fold is shown to be intact without failure.

laser heating, which has the advantage of offering rapid energy delivery with precise control of fluence dose and location of heating, with rastering underscores the versatility of our technique. Among folding-based methods, our approach uniquely allows optimizing the folding angle and minimizing hinge distortion when compared with less abrupt heating methods [9,12]. Another advantage for our approach is that folding happens as a result of a single-step direct-write process, eliminating the need for ink printing. However, further process development is needed to achieve more complex 3D geometries [21], since shadowing effects can potentially limit the maximum achievable folds and block the laser when lasing large structures. These issues can potentially be remedied by using different scanning methods like using mirror galvanometers to deliver the laser energy fast-enough before shadowing can occur. The approach of directed self-folding based on localized heating can be combined with modern cybermanufacturing infrastructure in order to achieve mass customization in 3D fabrication at on-demand stations or kiosks [28,29].

4 Conclusion

In this work, we present a new approach for sequential self-folding of polymer sheets, based on laser rastering. The approach is shown to be versatile, allowing direct precise delivery of energy at the folds, without the need for ink jet printing to sequentially fold the pre-strained polymer sheets. This approach is well suited for creating complex shapes that are difficult to create with 3D printing techniques. From the parametric study results, it is noted that varying the number of lasing passes is a powerful way to achieve high-quality folds with desired angles. Additionally, it is observed that power and speed represent a direct method for controlling the folding angle while maintaining the quality of the fold. Our findings indicate that optimal conditions exist, which insure both minimal distortion in fold geometries and high precision in the resulting folding angle. Further investigations are needed to correlate the lasing parameters with the spatial variation of fluence and temperature, as well as with the viscoelastic stress relaxation behavior that underlie folding. Taken together, our results highlight the potential of this approach for manufacturing 3D lightweight structures.

Acknowledgment

This research was supported by the National Science Foundation (NSF) under award number 2028580 (any opinions, findings, and conclusions or recommendations expressed in this material are those of the author(s) and do not necessarily reflect the views of the National Science Foundation). Work was also supported by the Department of Industrial Engineering at the University of Pittsburgh. J. Line was supported by the Allias/Holzman Fellowship through the Swanson School of Engineering undergraduate program.

Conflict of Interest

There are no conflicts of interest.

Data Availability Statement

The datasets generated and supporting the findings of this article are obtainable from the corresponding author upon reasonable request. The authors attest that all data for this study are included in the paper. Data provided by a third party listed in Acknowledgment.

References

[1] Kellermayer, M. S. Z., Smith, S. B., Granzier, H. L., and Bustamante, C., 1997, "Folding-Unfolding Transitions in Single Titin Molecules Characterized With Laser Tweezers," Science, **276**(5315), pp. 1112–1116.
[2] Saito, K., Nomura, S., Yamamoto, S., Niiyama, R., and Okabe, Y., 2017, "Investigation of Hindwing Folding in Ladybird Beetles by Artificial Elytron Transplantation and Microcomputed Tomography," Proc. Natl. Acad. Sci. U. S. A., **114**(22), pp. 5624–5628.
[3] Todd, P. H., 1982, "A Geometric Model for the Cortical Folding Pattern of Simple Folded Brains," J. Theor. Biol., **97**(3), pp. 529–538.
[4] Mahadevan, L., and Rica, S., 2005, "Self-Organized Origami," Science, **307**(5716), p. 1740.
[5] Felton, S., Tolley, M., Demaine, E., Rus, D., and Wood, R., 2014, "A Method for Building Self-Folding Machines," Science, **345**(6197), pp. 644–646.
[6] Yakacki, C. M., Shandas, R., Lanning, C., Rech, B., Eckstein, A., and Gall, K., 2007, "Unconstrained Recovery Characterization of Shape-Memory Polymer Networks for Cardiovascular Applications," Biomaterials, **28**(14), pp. 2255–2263.
[7] Morgan, J., Magleby, S. P., and Howell, L. L., 2016, "An Approach to Designing Origami-Adapted Aerospace Mechanisms," ASME J. Mech. Des., **138**(5), p. 052301.
[8] Song, Z., Ma, T., Tang, R., Cheng, Q., Wang, X., Krishnaraju, D., Panat, R., Chan, C. K., Yu, H., and Jiang, H., 2014, "Origami Lithium-Ion Batteries," Nat. Commun., **5**, p. 3140 .
[9] Elsisy, M., Poska, E., and Bedewy, M., 2018, "Current-Dependent Kinetics of Self-Folding for Multi-Layer Polymers Using Local Resistive Heating," Proceedings of the 2018 Manufacturing Science and Engineering Conference, College Station, TX, June 18–22, p. V002T04A017.
[10] Elsisy, M., Poska, E., Abdulhafez, M., and Bedewy, M., 2021, "Current-Dependent Dynamics of Bidirectional Self-Folding for Multi-Layer Polymers Using Local Resistive Heating," ASME J. Eng. Mater. Technol., pp. 1–26.

[11] Cho, J. H., Azam, A., and Gracias, D. H., 2010, "Three Dimensional Nanofabrication Using Surface Forces," Langmuir, **26**(21), pp. 16534–16539.
[12] Liu, Y., Boyles, J. K., Genzer, J., and Dickey, M. D., 2012, "Self-Folding of Polymer Sheets Using Local Light Absorption," Soft Matter., **8**(6), p. 1764.
[13] Felton, S. M., Tolley, M. T., Shin, B., Onal, C. D., Demaine, E. D., Rus, D., and Wood, R. J., 2013, "Self-Folding With Shape Memory Composites," Soft Matter, **9**(32), pp. 7688–7694.
[14] Mueller, S., Kruck, B., and Baudisch, P., 2013, "LaserOrigami," CHI '13 Extended Abstracts on Human Factors in Computing Systems on—CHI EA '13, Paris, France, Apr. 27–May 2, ACM Press, New York, NY, p. 2851.
[15] Liu, Y., Shaw, B., Dickey, M. D., and Genzer, J., 2017, "Sequential Self-Folding of Polymer Sheets," Sci. Adv., **3**(3), pp. 1–7.
[16] Davis, D., Mailen, R., Genzer, J., and Dickey, M. D., 2015, "Self-Folding of Polymer Sheets Using Microwaves and Graphene Ink," RSC Adv., **5**(108), pp. 89254–89261.
[17] Suzuki, K., Yamada, H., Miura, H., and Takanobu, H., 2007, "Self-Assembly of Three Dimensional Micro Mechanisms Using Thermal Shrinkage of Polyimide," Microsyst. Technol., **13**(8–10), pp. 1047–1053.
[18] Piqué, A., Mathews, S. A., Charipar, N. A., and Birnbaum, A. J., 2012, "Laser Origami: A New Technique for Assembling 3D Microstructures," Laser-based Micro- Nanopackaging Assem. VI. Proc. SPIE, **8244**, p. 82440B.
[19] Tolley, M. T., Felton, S. M., Miyashita, S., Aukes, D., Rus, D., and Wood, R. J., 2014, "Self-Folding Origami: Shape Memory Composites Activated by Uniform Heating," Smart Mater. Struct., **23**(9), p. 094006.
[20] Lee, J. G., Won, S., Park, J. E., and Wie, J. J., 2020, "Multifunctional Three-Dimensional Curvilinear Self-Folding of Glassy Polymers," J. Micro Nano-Manuf., **8**(3), pp. 1–7.
[21] Lee, J. H., Choi, J. C., Won, S., Lee, J. W., Lee, J. G., Kim, H. R., and Wie, J. J., 2020, "Light-Driven Complex 3D Shape Morphing of Glassy Polymers by Resolving Spatio-Temporal Stress Confliction," Sci. Rep., **10**(1), pp. 1–12.
[22] Liu, Y., Miskiewicz, M., Escuti, M. J., Genzer, J., and Dickey, M. D., 2014, "Three-Dimensional Folding of Pre-Strained Polymer Sheets via Absorption of Laser Light," J. Appl. Phys., **115**(20), p. 204911.
[23] Bilger, H. R., and Habib, T., 1985, "Knife-Edge Scanning of an Astigmatic Gaussian Beam," Appl. Opt., **24**(5), p. 686.
[24] Callens, S. J. P., Tümer, N., and Zadpoor, A. A., 2019, "Hyperbolic Origami-Inspired Folding of Triply Periodic Minimal Surface Structures," Appl," Mater. Today, **15**, pp. 453–461.
[25] Lamoureux, A., Lee, K., Shlian, M., Forrest, S. R., and Shtein, M., 2015, "Dynamic Kirigami Structures for Integrated Solar Tracking," Nat. Commun., **6**(1), pp. 1–6.
[26] Xiang, X. M., Lu, G., and You, Z., 2020, "Energy Absorption of Origami Inspired Structures and Materials," Thin-Walled Struct., **157**, p. 107130.
[27] Kamrava, S., Mousanezhad, D., Ebrahimi, H., Ghosh, R., and Vaziri, A., 2017, "Origami-Based Cellular Metamaterial With Auxetic, Bistable, and Self-Locking Properties," Sci. Rep., **7**(1), pp. 1–9.
[28] Wang, Z., Iquebal, A. S., and Bukkapatnam, S. T. S., 2018, "A Vision-Based Monitoring Approach for Real-Time Control of Laser Origami Cybermanufacturing Processes," Procedia Manuf., **26**, pp. 1307–1317.
[29] Iquebal, A. S., Wang, Z., Ko, W. H., Wang, Z., Kumar, P. R., Srinivasa, A., and Bukkapatnam, S. T. S., 2018, "Towards Realizing Cybermanufacturing Kiosks: Quality Assurance Challenges and Opportunities," Procedia Manuf., **26**, pp. 1296–1306.